PHYSICAL REVIEW A VOLUME 16, NUMBER 1 JULY 1977

# Electron-impact excitation of helium: Cross sections, $n$, and $l$ distributions of high Rydberg states

James A. Schiavone, David E. Donohue, David R. Herrick,* and Robert S. Freund
*Bell Laboratories, Murray Hill, New Jersey 07974*
(Received 31 January 1977)

Helium atoms in highly excited Rydberg states are produced by electron impact and are detected by electric field ionization. The principal quantum numbers $n$ are determined to lie in the range $20 \lesssim n \lesssim 80$ by ionizing the excited He atoms in a uniform, swept electric field. The absolute excitation cross section for 100-eV incident electrons is found to be $(9 \pm 5) \times 10^{-17}/n^3$ cm$^2$. This expression predicts a value for $n = 4$ that agrees with the optically measured $n = 4$ cross section. The 108-$\mu$sec time of flight requires that the high Rydberg He atoms have lifetimes much longer than those calculated for low-angular-momentum ($l \leq 2$) states, those expected to be populated by electron impact. The proposed explanation is that the excited He atoms suffer collisions with electrons and/or ground-state He atoms causing longer-lived higher $l$ states to be populated. This explanation is supported by measurements of signal as a function of incident-electron energy, electron current, and He pressure. The cross section for $l$-changing collisions between electrons and high Rydberg helium atoms is given by $\sigma^c_{\Delta l} \cong 5 \times 10^{-(15 \pm 0.3)} \ln(100En^2) n^4/E$ cm$^2$.

## I. INTRODUCTION

Highly excited Rydberg states (HR) have been studied in the laboratory by a variety of methods, including electron transfer,[1-3] photoexcitation,[4-7] and more recently by laser excitation.[8-15] An additional method, electron impact, has been used extensively in the past decade to study various properties of HR states. Čermák and Herman[16] studied mechanisms by which HR rare-gas atoms could be detected, and also measured He and Ar signals as a function of incident electron energy (excitation functions). Kupriyanov[17-20] measured excitation functions for rare gases and for atomic fragments resulting from dissociative excitation of diatomic molecules. Hotop and Niehaus[21,22] and Sugiura and Arakawa[23] studied ionization of molecules by collisions with HR rare-gas atoms. Freund *et al.*[24-27] and Zipf *et al.*[28-30] studied dissociative excitation processes in small molecules. For some electron impact experiments estimates have been made of the ranges of principal quantum numbers detected and of absolute excitation cross sections.[31,32] However, no accurate measurements of these properties have been reported.

In the present work, we measure the distribution of principal quantum states of helium, excited by low-energy electron impact. These principal quantum number distributions are acquired by ionizing the excited He atoms in a uniform, controllable electric field. We find that the detected atoms have $n$ values in the range 20–80. We also measure the absolute excitation cross section for the detected HR He atoms, $\sigma^{ex}$. From both of these measurements we determine the absolute cross sections for excitation of individual $n$ levels, $\sigma^{ex}(n)$. Extrapolation of these results down to $n = 4$ gives a cross section in excellent agreement with the $n = 4$ cross section measured via optical emission.[33]

A key feature of our analysis is that, because of radiative decay, very few of the low-$l$ Rydberg atoms having $n < 50$ ever reach the detector. Low-$l$ states ($S, P, D$) are thought to dominate in the initial electron impact excitation. The observed detector signal, however, shows a substantial number of atoms having $n < 50$, much larger than could be expected from low-$l$ atoms alone. We propose, therefore, a model wherein high-$l$ states are populated via collisions of low-$l$ Rydberg atoms with either electrons or ground-state He atoms. The resulting high-$l$ states do not suffer appreciable radiative decay during the time of flight to the detector, and can thus account for observed signal. From measurements of the HR signal as a function of four variables (principal quantum number, incident electron energy, electron current, and helium pressure) we conclude that angular momentum changes resulting from electron collisions dominate the present experiments. The required cross sections for collision of electrons with high Rydberg atoms are huge—of the order of $10^6$ Å$^2$. We therefore devise procedures to measure these cross sections approximately and discuss the mechanism which can lead to such large values.

## II. APPARATUS

High Rydberg atoms are formed by collisions of electrons with He atoms. A small fraction of them head toward the detector (Fig. 1), located 20.1 cm from the electron beam. The mean time of flight to the detector, $t_d$, is 108 $\mu$s. Charged particles are kept from the detector by an ion extractor.

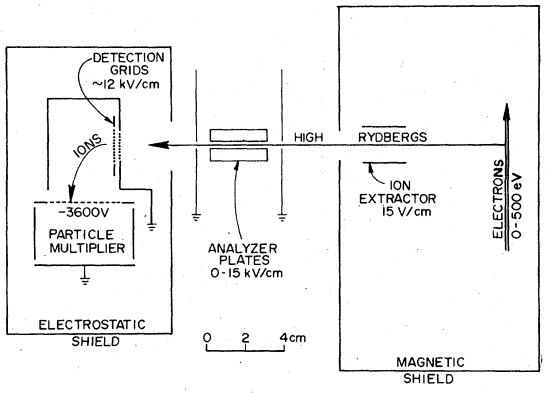


FIG. 1. Apparatus.

Time of flight is used to separate HR atoms from photons whenever necessary.

Measurements that do not require quantum state analysis are made with this form of the apparatus. The addition of analyzer plates provides for electric field ionization of high Rydbergs in a uniform field and permits a determination of the principal quantum number distribution.

Two different electron guns were used in these experiments. Most data were acquired with an ARIS model ESA 1000 Pierce-type electron gun, which is described more fully in Ref. 25. A simpler gun with a planar nickel matrix oxide cathode[34] and two planar grids was employed to check and acquire some absolute cross-section measurements and excitation functions. It does not focus the electron beam and maintains all potentials in the gun below the final electron energy. Energy spreads for both guns are about 300 meV for 50% of the electrons, as determined by measurements of sharp thresholds and the excitation function for metastable He atoms. Current to the Faraday cup is usually maintained at 30 $\mu$A. The electron beam diameter is about 2 mm with the ARIS gun and 6 mm with the planar gun.

Gas is admitted to the vacuum chamber at a location outside the magnetic shield which insures a uniform He density over the electron beam and flight regions. Pressure is usually maintained at $\leq 10^{-5}$ Torr; its measurement is discussed in Sec. IV C.

The analyzing electric field is created by a pair of 3-cm-long 4-cm-wide stainless-steel flat parallel plates, separated by $0.317 \pm 0.004$ cm. A pair of 0.25-cm wide collimating slits, which also serve as grounded electrostatic shields, are located at the entrance and exit of the analyzing region. High Rydbergs are therefore kept at least 0.03 cm from the plate surfaces, so they are not exposed to microscopic field variations. The maximum available electric field is 15.7 kV/cm. As high Rydbergs pass through this field, those with sufficiently high $n$ are field ionized. The resulting ions and electrons are removed by the electric field. The transmitted HR signal, as a function of electric field, is called a transmission function (Fig. 2). Signal is accumulated in the memory of a PDP8/L computer which also repetitively sweeps the electric field via a digital-to-analog converter and a Kepco OPS 5000 operational power supply.

A high Rydberg detector was previously devised for work on dissociation of $N_2$, CO, and $H_2$.[25-27] HR atoms which passed through a grid were detected by two mechanisms, resonance ionization and field ionization. Resonance ionization[16,35,36] occurred as some of the highly excited species passed very close to the wires of the entrance grid; the resultant ions were collected by the first dynode of a Johnston Laboratories MM-1 particle multiplier. Additional high Rydbergs, which were not ionized at the entrance grid, were field ionized in the ~800 V/cm field between the first dynode of the multiplier, at -4 kV, and the grounded detector box. The lowest principal quantum state ionized by this field was $n \approx 30$.

For the present experiments we have improved the detector so that resonance ionization is unimportant compared to field ionization and so that we can detect quantum states lower than $n = 30$ with better sensitivity. In the new design, we have replaced the single entrance grid by two coarser grids (200 cells/in and 75% transparent vs 1500 cells/in for the previous detector) separated ~1 mm from each other. A negative 1-kV potential is applied to the second grid; the entrance grid, to-

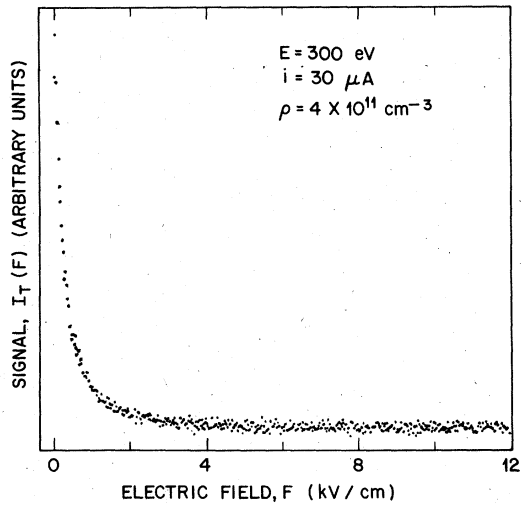


FIG. 2. Typical transmission function: detected high Rydberg He signal measured as a function of analyzer electric field.

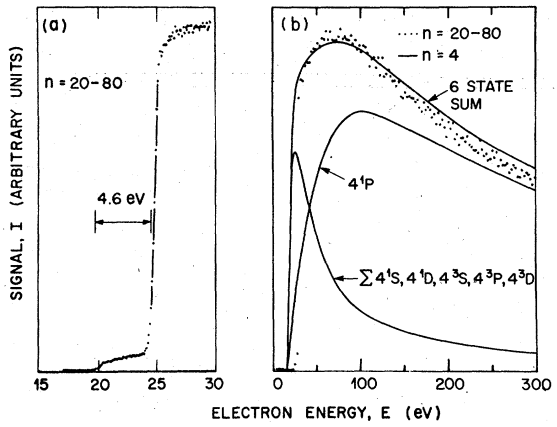


FIG. 3. Excitation functions for He Rydberg states. (a) Threshold region showing detection of both metastables and high Rydbergs and the measured energy difference between their appearance potentials. High Rydberg threshold region cross sections (relative to the peak in the $n = 20$–$80$ excitation function) are 0.18 at 24.6 eV, 0.38 at 24.8 eV, 0.61 at 25.0 eV, and 0.72 at 25.2 eV. (b) Comparison of the high Rydberg excitation function with $n = 4$ excitation functions measured optically by Donohue *et al.* (Ref. 33). The absolute cross section at $E = 100$ eV for the six-state sum is $1.2 \times 10^{-18}$ cm$^2$ (Ref. 33). The $n = 4$ curves are drawn with the correct relative scale. The $4\,^1P$, five-state sum and six-state sum peak, respectively, at 100, 26, and 73 eV.

gether with the detector box, is at ground potential. This design works in the following way: Highly excited species in principal quantum states down to $n \approx 15$ are field ionized in the ~12 kV/cm field between the two entrance grids and are accelerated into the detector box. The resultant ions are drawn to the first dynode of the particle multiplier at −3600 V, but cannot strike the grounded surfaces. Thus, except for ions which strike the wires of the inner grid, this design should be 100% efficient. When we account for the area of the grid wires, a more realistic estimate of the detector efficiency $\eta$ is $(60 \pm 10)\%$. Resonance ionization takes place with this design, also, but should be much less important than electric field ionization due to the coarse grids and the large electric field.

The present detector (just as the previous detector) is insensitive to ground-state particles and sees no charged particles because of deflecting fields in front of it. Metastable particles and uv photons (from electron collisions with the sample gas) can eject electrons from the grounded inside surfaces of the box, but these electrons cannot reach the multiplier at −3600 V. As there is no straight-line path from the interaction region to the multiplier, the only photons and metastables which are detected are those which survive at least one reflection (an improbable event) and strike the multiplier. Thus, although photons and metastables are much more numerous than HR atoms, their signals are weaker than the HR signals. Figure 3(a) shows the threshold regions for both metastable and HR He atoms. The separation of these two thresholds, 4.6 eV, agrees very well with the difference between the He ionization potential and the excitation energy for He metastables ($24.6 - 19.8 = 4.8$ eV). Since ions are carefully removed, this is an excellent confirmation that the major species we detect is indeed HR atoms. From the relative intensities of high Rydberg and metastable signals in Fig. 3(a) and from the absolute cross sections for producing metastable helium[37] and helium HR (see below), we calculate that this detector is ~4000 times more sensitive to HR He atoms than to helium metastables.

## III. PHENOMENOLOGICAL MODEL

In this section we first discuss processes affecting the angular momentum ($l$) states of excited helium atoms from the time of initial excitation to the time they reach the detector. Next we develop an expression for the detected signal $I(n, E, i, \rho)$ as a function of the principal quantum number $n$, the electron energy $E$, the current $i$, and the gas density $\rho$. We then simplify this general expression to apply to the specific experiments described herein.

### A. Processes affecting $l$ states

The initial electron-impact excitation to a HR state should involve a small change in $l$. Fano[38] has argued that large changes in $l$ are likely to occur only very near threshold (within 0.2 eV) where the scattered electron and excited electron are strongly correlated. This criterion for large $\Delta l$ upon excitation is not met in our experiments where incident electron energies are at least 1 eV above threshold. In addition, the Ochkur approximation[39] for singlet-triplet excitation shows that for exchange processes $\Delta l = 0$ is the preferred transition, and that $\Delta l \geq 2$ is not likely. We expect, therefore that the initial excitation produces HR states with low angular momenta, these being predominately $^{1,3}S$, $^{1,3}P$, and $^{1,3}D$.

Once the high Rydberg atom is formed it can radiate or it can collide with another particle. Collisions with electrons, we find below, are of great importance. Under the present experimental conditions, namely, the electron-HR collision energy is many times the threshold energy, Seaton's impact parameter approximation[40] should be applicable. In the dipole level of this approximation,

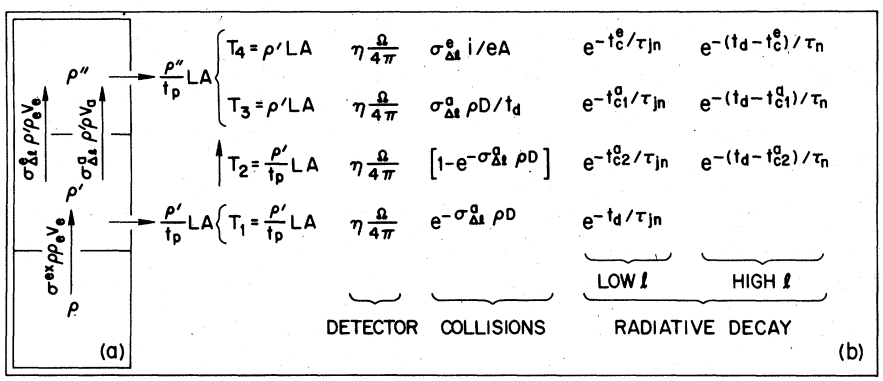


Fig. 4. Summary of processes affecting He high Rydberg atoms: (a) collisions with electrons and atoms within the electron beam, and (b) collisions with atoms and radiative decay during flight to the detector. In (a) densities of He atoms in ground, low $l$ high $n$, and high $l$ high $n$ states are represented by $\rho$, $\rho'$, and $\rho''$, respectively. The three important rate constants between these three groups are indicated by the vertical arrows. The rates at which high Rydbergs leave the electron beam region are approximated by $\rho' LA/t_p$ and $\rho'' LA/t_p$. In (b) the 4 contributions ($T_1, T_2, T_3, T_4$) to the detected high Rydberg signal are shown (where each term is given by the product of factors to its right). $T_1$ and $T_2$ include collisions with atoms only outside the electron beam while $T_3$ and $T_4$ include collisions with atoms and electrons only inside the electron beam.

the transition probability between two states is calculated by time-dependent perturbation theory, the Coulomb interaction is expanded and only the electric dipole term kept. The cross section is then derived by integrating over all impact parameters. In the high collision-energy limit, the resulting cross section is proportional to the optical oscillator strength $f_{n'l',nl}$. Since $f_{n'l',nl}$ is proportional to the square of the transition moment and the transition moment is proportional to the square of the principal quantum number $n$, the cross section is approximately proportional to $n^4$ when $n' \simeq n$. The general high-energy form of the cross section, which we call $\sigma^e_{\Delta l}$, can be written

$$\sigma^e_{\Delta l} = (Kn^4/E)\ln(\gamma n^2 E)\,, \tag{1}$$

where $E$ is the collision energy in eV and $K$ and $\gamma$ are constants. For $n = n'$, this expression has also been considered by Pengelly and Seaton[41] and evaluated by Herrick.[42] For $n' = n \pm 1$, Saraph[43] has reported numerical values of the cross section. These calculations show that the cross sections for $\Delta n = 0$ are about ten times larger than those for $\Delta n = \pm 1$.

Collisions with ground-state He atoms offer a second way for changing $n$ or $l$ in the HR atom. Because $\Delta n$ transitions could be large for collisions with atoms, both $\Delta n$ transitions and ionization will be designated as atomic quenching interactions with symbolic cross section $\sigma^a_q$. Cross sections for $\Delta l$ transitions caused by atomic collisions are designated $\sigma^a_{\Delta l}$. Collisions with ions or other high Rydberg atoms are relatively unlikely due to the low density of these species.

### B. Development of a signal intensity formula

The observed signal $I(n, E, i, \rho)$ is interpreted by a model which is admittedly oversimplified, but which should be capable of representing the observations. Processes occurring within the electron beam are expressed in terms of three effective states, one which is ground-state atoms, a second which represents HR states with low $l$ and therefore short radiative lifetimes, and a third which represents HR states with high $l$ and therefore long radiative lifetimes. The three boxes in Fig. 4(a) represent densities of He atoms in the ground state ($\rho$), in HR states with low $l$ ($\rho'$), and in HR states with high $l$ ($\rho''$) as labeled. In addition to the three collision processes shown we assume that excited atoms leave the electron beam region at rates $\rho' LA/t_p$ and $\rho'' LA/t_p$. $L$ is the electron-beam length viewed by the detector, $A$ is the electron beam area, and $t_p$ is the mean time after excitation for the atom to reach the perimeter of the electron beam in the direction of the detector, traveling at thermal velocity. The steady-state approximation for HR atoms within the electron beam yields the rate equations

$$\frac{d\rho'}{dt} = \sigma^{ex}\rho\rho_e v_e - \sigma^e_{\Delta l}\rho'\rho_e v_e - \sigma^a_{\Delta l}\rho'\rho v_a - \rho'/t_p - \rho'/\tau_{nj} = 0\,, \tag{2}$$

$$\frac{d\rho''}{dt} = \sigma^e_{\Delta l}\rho'\rho_e v_e + \sigma^a_{\Delta l}\rho'\rho v_a - \rho''/t_p = 0\,. \tag{3}$$

Here $\sigma^{ex}$ is the excitation cross section for low-$l$ Rydberg atoms, $\rho_e$ is the electron density, and $v_e$

and $v_a$ are the electron and He-atom velocities. $\rho'/\tau_{nj}$ represents the effective radiative loss of low-$l$ atoms before they leave the electron beam. Radiative decay of high-$l$ atoms during the short time they are in the electron beam is assumed to be negligible. In this model, $\sigma_{\Delta l}$ is not precisely defined; it represents an average over all $\Delta l$ processes. In the absence of radiative decay and collisions outside of the electron beam, the total HR signal detected would be

$$I = LA\eta\frac{\Omega}{4\pi}\sum_{j,n}\left(\frac{\rho'}{t_p}+\frac{\rho''}{t_p}\right), \tag{4}$$

where $\Omega$ is the detector solid angle, $\eta$ is the detector efficiency, and $j$ represents one of the singlet or triplet $S$, $P$, or $D$ states. $\rho'/t_p$ and $\rho''/t_p$ are easily obtained from Eqs. (2) and (3):

$$\frac{\rho'}{t_p} = \frac{\sigma^{ex}\rho i/eAt_p}{\sigma^e_{\Delta l} i/eA + \sigma^a_{\Delta l}\rho D/t_d + 1/t_p + 1/\tau_{nj}}, \tag{5}$$

$$\frac{\rho''}{t_p} = \rho'\left(\frac{\sigma^e_{\Delta l} i}{eA}+\frac{\sigma^a_{\Delta l}\rho D}{t_d}\right). \tag{6}$$

We have used the substitutions $\rho_e v_e = i/eA$ and $v_a = D/t_d$, where $e$ is the electron charge and $D = 20.1$ cm, the distance to the detector.

We now examine processes affecting the excited atoms during their flight to the detector, radiative decay and collisions with ground-state He atoms. Consider first the contribution from low-$l$ Rydberg atoms, Eq. (5). A fraction of them, $1 - \exp(-\sigma^a_{\Delta l}\rho D)$, may suffer collisions which cause angular momentum changes $\Delta l$. For the moment we assume that the $\Delta l$ in one collision is sufficient to shift the Rydberg atom from the low-$l$ regime (short radiative lifetime) to the high-$l$ regime (long radiative lifetime). Those that do not collide will decay radiatively by $\exp(-t_d/\tau_{nj})$ where $t_d$ is the mean time of flight to the detector (108 $\mu$s) and $\tau_{nj}$ is the radiative lifetime for a particular substate $j$ of a given level $n$. Those that do collide decay radiatively by this same decay factor until the time of collision $t^a_{c2}$. Thereafter, a longer lifetime $\tau_n$ independent of substate is assumed to be applicable for the high-$l$ Rydberg states. These contributions to the detected signal for a given $j$ substate and $n$ level are identified as $T_1$ and $T_2$ in Fig. 4(b).

Next consider the contribution of high-$l$ Rydberg atoms to the detected signal, Eq. (6). An atom initially in a low-$l$ state decays radiatively with a lifetime $\tau_{nj}$ until the time $t^e_c$ at which it collides with an electron and undergoes a transition to a higher $l$ state [first term in Eq. (6)]. Similarly, radiative decay occurs for the second term in Eq. (6) with the same lifetime $\tau_{nj}$ applicable but until the time of collision $t^a_{c1}$ of the low-$l$ HR with a neutral atom within the electron beam. These contributions for a given $j$ substate and $n$ level are identified as $T3$ and $T4$ in Fig. 4(b).

Finally, a factor for quenching of all Rydberg atoms (high or low $l$) by collisions with neutral atoms is introduced for all four terms in Fig. 4 as $\exp(-\sigma^a_q\rho D)$. The equation for the number of HR atoms in level $n$ that reaches the detector per unit time can now be written

$$I(n,E,i,\rho) = \sum_j (T_1+T_2+T_3+T_4)\exp(-\sigma^a_q\rho D), \tag{7}$$

where the summation is over the substates with $l \leq 2$. The $E$ dependence arises from the initial excitation cross section, $\sigma^{ex}(E)$.

Variables $L$, $A$, $D$, $n$, and $\Omega$ are obtained by primary experimental measurements. We estimate $t_p \approx t_d R/D$, where $R \approx 0.1$ cm, the radius of the electron beam. Radiative lifetimes, $\tau_{nj}$, for low-$l$ Rydberg He atoms can be extrapolated from oscillator strength calculations.[44] The time before collision of a low-$l$ Rydberg atom with an electron is estimated by $t^e_c \approx Ae/i\sigma^e_{\Delta l}$. The time before collision with a neutral atom is estimated by $t^a_c \approx t_d/\sigma^a_{\Delta l}\rho D$. Because collisions with atoms occur both within and outside the electron beam the restrictions $0 \leq t^a_{c1} \leq t_p$ and $t_p \leq t^a_{c2} \leq t_d$ apply. $c1$ and $c2$ designate collisions within and outside the electron beam, respectively. $\sigma^{ex}$ will be left unspecified for the moment.

### C. Simplification of the general expression

We now anticipate the experimental results to simplify Eq. (7). Quantitative verification will be obtained in Sec. IV D.

In the present experiments, contributions from $T1$ and $T3$ [Fig. 4(b)] are not important. These terms apply to low-$l$ Rydberg atoms which suffer no collisions, or collide with ground-state atoms within the electron beam. From Eqs. (5) and (7) and Fig. 4 we therefore obtain the following:

$$I(n,E,i,\rho) = \frac{\eta L\Omega\rho i/4\pi e t_p}{\sigma^e_{\Delta l} i/eA + \sigma^a_{\Delta l}\rho D/t_d + 1/t_p + 1/\tau_{nj}}\exp(-\sigma^a_q\rho D)$$
$$\times\sum_j \sigma^{ex}\left[\left(\frac{t_p\sigma^e_{\Delta l} i}{eA}\right)\exp\left(-\frac{t^e_c}{\tau_{nj}}-\frac{t_d}{\tau_n}+\frac{t^e_c}{\tau_n}\right)+[1-\exp(-\sigma^a_{\Delta l}\rho D)]\exp\left(-\frac{t^a_{c2}}{\tau_{nj}}-\frac{t_d}{\tau_n}+\frac{t^a_{c2}}{\tau_n}\right)\right]. \tag{8}$$

Equation (8) will be used to estimate $\sigma^a_{\Delta l}$ and $\sigma^a_q$. For He pressures $\lesssim 5\times10^{-5}$ Torr, $\exp(-\sigma^a_q\rho D)$ and

$\exp(-\sigma^a_{\Delta l}\rho D)$ are nearly unity, and $t^e_c \ll t_d$, so Eq. (8) reduces to

$$I(n,E,i,\rho) = \frac{(\sigma^e_{\Delta l} i/eA)\eta L\Omega\rho i/4\pi e}{\sigma^e_{\Delta l} i/eA + \sigma^a_{\Delta l}\rho D/t_d + 1/t_p + 1/\tau_{nj}} \sum_j \sigma^{ex} \exp\left(-\frac{t^e_c}{\tau_{nj}} - \frac{t_d}{\tau_n}\right). \quad (9)$$

Equation (9) will be used to determine $\sigma^e_{\Delta l}$. Determination of the principal quantum number distributions requires application of a least squares fitting procedure to the appropriate data. Since most of these experiments were performed under conditions ($i > 30$ $\mu$A) such that $\sigma^e_{\Delta l}\, i/eA$ is large compared to the other three terms in the denominator of Eq. (9), and also $\exp[-t^e_c/\tau_{jn} - t_d/\tau_n] \approx \exp(-t_d/\tau_n)$, Eq. (9) becomes simply

$$I(n,E,i,\rho) = \frac{\eta L\Omega\rho i}{4\pi e}\, \sigma^{ex}(n,E) \exp\left(-\frac{t_d}{\tau_n}\right). \quad (10)$$

Notice that when $n$ distributions are measured using Eq. (10) values of $\tau_n$, representing an effective radiative lifetime for all high $l$ states, are also determined in the process.

Finally, we set

$$\sigma^{ex}(n,E) = \sigma^{ex}(n=1,E)n^{-3} \quad (11)$$

in accordance with the usual assumptions of Rydberg orbital overlap with the ground state. This form is valid for all $l \ll n$ and is not restricted to optically allowed transitions, an important factor when excitation is produced by low-energy electron impact.

## IV. RESULTS AND DISCUSSION

In this section we first discuss measurement techniques, present data, and make comparisons with data from other experiments. We then analyze these results using Eqs. (8) and (9) to obtain the high Rydberg collision cross sections $\sigma^e_{\Delta l}$, $\sigma^a_{\Delta l}$, and $\sigma^a_q$. Table I lists the types of measurements we have performed and the results sought by each.

### A. $n$ distributions from field ionization

Before reaching the detector the He atoms pass through an electric field analyzer (c.f. Fig. 1). The Stark field, $F$, selectively ionizes atoms according to their principal quantum number. The critical field for ionization of a HR hydrogen atom is

$$F = C/n^4, \quad (12)$$

where $C$ is characteristic of the individual Stark energy-level components. Classical energy considerations alone predict $C = \frac{1}{16}$ a.u., or $C = 3.2 \times 10^8$ V/cm, for all components of level $n$. Although ionization is expected to occur at lower fields due to tunneling, the separability of the hydrogen-atom wave function in parabolic coordinates tends to shift the critical field instead to higher values. Herrick[45] has estimated from quantum mechanical calculations that the lowest-energy Stark component has $C = 5.1 \times 10^8$ V/cm, while the corresponding classical value is $C = 6.2 \times 10^8$ V/cm. The higher Stark components for each $n$ have slightly larger values of $C$, a shift which is reflected in values determined from experiments involving mixtures of Stark states as shown in Table II. Similar, but noisy measurements have been made by electron impact in this laboratory yielding results consistent with those obtained for production of HR atoms by electron capture and charge exchange. For atoms other than hydrogen both large quantum defects for low-$l$ states and also level crossings give rise to a more complicated spectrum as $F$ is varied,[15] leading to slightly different values of $C$ shown in Table II.

TABLE I. Guide to the measurements of high Rydberg signal $I$ as a function of the experimental variables of electron energy $E$, electron current $i$, helium-gas density $\rho$, and principal quantum number $n$. These measurements give values of lifetime $\tau$ and various cross section $\sigma$ as defined in the text.

| Dependent variable | Independent variable | Varied parameters | Fixed parameters | Results sought | Figure |
|---|---|---|---|---|---|
| $I$ | $n$ | $E,\rho$ | $i = 30$ $\mu$A | $\tau_n$ | 5 |
| $I$ | $E$ | $n,\rho$ | $i = 30$ $\mu$A | $\sigma^e_{\Delta l}$ | 6 |
| $I$ | $i$ | $n,E$ | $\rho = 2\times10^{11}$ cm$^{-3}$ | $\sigma^e_{\Delta l}$ | 8(a), 8(b) |
| $I$ | $\rho$ | $n,E$ | $i = 30$ $\mu$A | $\sigma^a_{\Delta l}$, $\sigma^a_q$ | 8(c), 8(d) |
| $\hat{I}$ | ... | $E,\rho$ | $15 \le n \le 80$<br>$i = 30$ $\mu$A | $\sigma^{ex}$ | ... |

TABLE II. Experimental values of field ionization proportionality constant for high Rydberg atoms. We obtain these values of $C$ from plots of $n$ vs $F$ given in the referenced works assuming the power of $n$ to be 4.

| Experimenters | Production mechanism | Atom studied | Principal quantum numbers observed | $C = Fn^4$ ($10^8$ V/cm) |
|---|---|---|---|---|
| This laboratory | Electron-impact dissociation | H | 15–19 | 6.3 |
| This laboratory | Electron-impact dissociation | N | 15–19 | 6.3 |
| Riviere and Sweetman [a] | Charge exchange | H | 9–22 | 6.5 |
| Il'in *et al.* [b] | Charge exchange | H | 9–16 | 6.8 |
| Il'in *et al.* [b] | Charge exchange | He | 9–17 | 5.8 |
| Bayfield *et al.* [c] | Charge exchange | H | 19–28 | 6.5 |
| Ducas *et al.* [d] | Laser excitation | Na | 26–37 | 3.1 |
| Stebbings *et al.* [e] | Laser excitation | Xe | 24–40 | 4.6 |

[a] Reference 50.
[b] Reference 1.
[c] Reference 3.
[d] Reference 14.
[e] Reference 8.

In our He experiments data are collected in the form of transmission functions, for which we measure high Rydberg signals as a function of ionizing electric field, $F$. An example is displayed in Fig. 2. We relate $n$ to $F$ with Eq. (12) using a value $C = 6 \times 10^8$ V/cm. The numerical analysis consists of first fitting the transmission function using Eqs. (10) and (11), and then converting from $I(F)$ to $I(n)$. $E$, $i$, and $\rho$ are constants for each $n$-distribution experiment. Hence, Eqs. (10) and (11) can be simplified to

$$I(n) = an^{-3} \exp(-t_d/\tau_n) , \tag{13}$$

with

$$a = \frac{\eta L \Omega \rho i}{4\pi e} \sigma^{ex}(n=1, E) . \tag{14}$$

The total Rydberg signal at the detector as a function of electric field can then be represented by

$$I_T(F) = \sum_{n=15}^{80} I(n) - \sum_{n=(C/F)^{1/4}}^{80} I(n) . \tag{15}$$

The first term is a constant, henceforth labeled $I_0$, representing the zero field signal. Virtually all states having $n < 15$ radiate before reaching the detector. Rydberg atoms with $n > 80$ are removed by the 15 V/cm electric field in the ion extractor.

We must now choose a model for $\tau_n$, the radiative lifetime of a particular principal quantum state. For fixed $l$ and large $n$, the lifetime is proportional to $n^3$. Since the data analysis presented deals only with populations in a given level $n$, summed over all $l$ and $S$, we must consider the effect of the $l$ distribution on the average lifetime for level $n$. For hydrogen, the statistical average lifetime for the $n$th quantum state is

$$\tau_n = \left( \sum_l \frac{2l+1}{n^2} \frac{1}{\tau_{n,l}} \right)^{-1} \propto n^{4.5} . \tag{16}$$

Thus we expect the choice $\tau_n = \tau_1 n^x$, where $3 \leq x \leq 4.5$ and $\tau_1$ is a variable parameter, to give reasonable results for our $l$ distributions. Substitution of $I(n)$, $I_0$, and $\tau_n$ into Eq. (15) with the aid of Eq. (13) yields

$$I_T(F) = I_0 - a \sum_{n=(C/F)^{1/4}}^{80} n^{-3} \exp(-t_d/\tau_1 n^x) , \tag{17}$$

which is our working model for the transmission functions.

We have determined parameters $I_0$, $a$, $\tau_1$, and $x$ from a nonlinear least-squares analysis of each transmission function $I(F)$. The resulting values for $I_0$ and $a$ have little significance because signal is not measured absolutely in the $n$-distribution experiments. Values of $\tau_1$ and $x$, which determine $\tau_n$, appear in Table III. They were found to be highly correlated in the fitting procedure and therefore do not have importance individually. We use the overall value $\tau_n$, however, in Eqs. (8) and (9) when measurements of $\sigma^e_{\Delta l}$, $\sigma^a_{\Delta l}$, and $\sigma^a_q$ are made.

Finally, we convert $I_T(F)$ to $I(n)$ by writing

$$I(n) = \frac{dI_T(n)}{dn} = \frac{dI_T(F)}{dF} \frac{dF}{dn} , \tag{18}$$

where $dF/dn = -4Cn^{-5}$ from Eq. (12). Principal quantum number distributions determined thusly using parameters from Table III appear in Figs. 5(a) and 5(b) for different values of $E$ and $\rho$, respectively. The curves decrease at low $n$ due to radiative decay, whereas the behavior at high $n$ is due to the $n^{-3}$ excitation cross-section dependence. The variations in shape for the different $E$ and $\rho$ curves will be discussed in Sec. IV D and IV E.

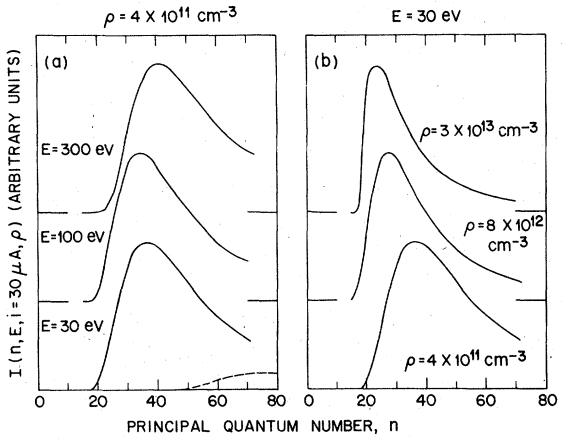


FIG. 5. He high Rydberg principal quantum number distributions measured at different electron energies in (a) and gas densities in (b). The dashed curve in the lower right corner of (a) is a distribution calculated assuming the absence of $l$-mixing collisions. This curve is scaled relative to the 30-eV curve.

TABLE III. Results of least squares fits to five different measured transmission functions. For different values of $E$ and $\rho$, the highly correlated variables $\tau_1$ and $x$ change significantly, so the resulting lifetimes $\tau_n = \tau_1 n^x$ are illustrated for $n = 20$ and 50. Some fall above and some below the most probable time of flight to the detector, 108 μsec.

| $E$ (eV) | $\rho$ ($10^{11}$ cm$^{-3}$) | $\tau_1$ (nsec) | $x$ | $n$ | $\tau_n$ (μsec) |
|---|---|---|---|---|---|
| 30 | 4 | 5.29 ± 2.20 | 2.73 ± 0.13 | 20 | 19 |
| | | | | 50 | 230 |
| 30 | 80 | 0.81 ± 0.24 | 3.61 ± 0.10 | 20 | 40 |
| | | | | 50 | 1100 |
| 30 | 300 | 0.35 ± 0.0007 | 4.11 ± 0.07 | 20 | 78 |
| | | | | 50 | 3360 |
| 100 | 4 | 2.08 ± 0.88 | 3.08 ± 0.13 | 20 | 21 |
| | | | | 50 | 355 |
| 300 | 4 | 1.03 ± 1.32 | 3.13 ± 0.39 | 20 | 12 |
| | | | | 50 | 214 |

### B. Excitation functions

Measured excitation functions for high Rydberg He atoms with $20 \leq n \leq 80$ are displayed in Figs. 3(a) and 3(b). In each case the analyzer was removed to accumulate greater signal. Three different $n$ ranges were also measured [Fig. 6(a)] by setting the ion extractor and detector grid voltages at the values shown in Table IV. For conciseness we refer to the different $n$ ranges by their median value, $\bar{n}$, as determined from Fig. 5. The three measurements illustrated in Fig. 6(b) show the excitation function dependence on the He density.

In Fig. 3(b) we compare the He excitation function for $20 \leq n \leq 80$ with the measured excitation function for $n = 4$ from Donohue *et al.*[33] Their curve labeled "6 state sum" is the sum of singlet and triplet $S$, $P$, and $D$ states. They also measured an excitation function for the $9^1P$ state and found that its shape agreed well with the $4\,^1P$-state curve. We thus have reason to expect that the $n = 4$ results may also be typical of those for $n > 20$. The comparison in Fig. 3(b) supports this notion. However, curves measured at either low $n$ or high pressure (Fig. 6) show deviations from this

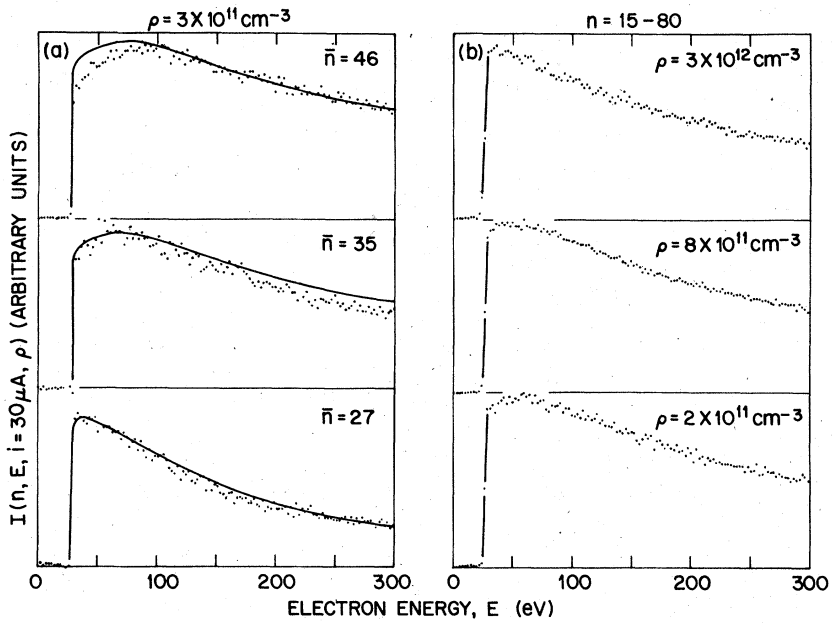


FIG. 6. He high Rydberg excitation functions measured for different $n$ ranges in (a) and gas densities in (b). The solid curves in (a) are excitation functions predicted by Eq. (8) with $\sigma^e_{\Delta l}$ given by Eq. (26) and $\sigma^{ex}(j, E)$ from excitation functions for $n = 4^{1,3}S$, $^{1,3}P$, and $^{1,3}D$ states measured in optical experiments by Donohue *et al.* (Ref. 33).

TABLE IV. Detector conditions which isolate specific $n$ ranges.

| Ion extractor (V/cm) | Detection grids (V/cm) | $n$ range | $\bar{n}$ for $E=100$ eV and $\rho=4\times10^{11}$ cm$^{-3}$ |
|---|---|---|---|
| 15 | 12 000 | 15–80 | ••• |
| 740 | 12 000 | 15–30 | 27±2 |
| 15 | 0 | 30–80 | 45±4 |
| 230 | 0 | 30–40 | 35±3 |
| By difference | | 40–80 | 52±4 |

shape due in large part to shifts in the contribution from the short-lived $^1P$ state. The $^1P$-state excitation function differs dramatically in shape from those of the $^1S$, $^1D$, $^3S$, $^3P$, and $^3D$ states[33] in that it peaks at ~100 eV compared to under 50 eV for the other five curves [Fig. 3(b)]. In addition, the absolute excitation cross section at the $^1P$ curve peak is much larger than those at the peaks for the other states. Thus the high Rydberg excitation-function shape appears to be highly sensitive to those experimental conditions which marginally prevent $^1P$ states from decaying radiatively. We will discuss this more fully in Sec. IV D.

High Rydberg He excitation functions measured by other workers[16–18,20,23] are compared in Fig. 7 to our curve for $20 \leq n \leq 80$. Our threshold is significantly more steep than in any previous measurement. The slower rises appearing in the previous work could be accounted for by large energy spreads in the exciting electron beams. In fact, the slope of the present measurement [Fig. 3(a)] may be due entirely to electron energy spread; the true threshold could be a step function, just as the threshold for excitation of the $2p$ state of atomic hydrogen is a step function, due to strong coupling between the $2s$ and $2p$ states.[46] Similar strong coupling could occur between the nearly degenerate $l$ states with sufficiently large $n$.

The differing shapes of the excitation functions in Fig. 7(b) are probably due to different experimental conditions. The shorter flight paths of previous workers permitted lower $n$ states to survive radiative decay and reach the detector. Collision with atoms and electrons can cause $l$ changes or quenching. Electric fields can ionize high $n$ states and mix $l$ levels in lower $n$ states. Unfortunately, the earlier papers give insufficient details to evaluate all of these conditions. It does appear, however, that it is meaningless to talk about *the* excitation function for HR atoms, unless the experimental conditions (or equivalently, the internal state distributions) are sufficiently well defined.

### C. Absolute excitation cross section

If we measure the total absolute high Rydberg signal $\hat{I}_T$ for a specified $n$ range, electron energy, and apparatus, Eq. (10) becomes

$$\hat{I}_T = \eta L \Omega \rho i \sigma_T^{ex}/4\pi e \,, \tag{19}$$

where

$$\sigma_T^{ex} \equiv \sum_n \sigma^{ex}(n,E) \exp(-t_d/\tau_n) \tag{20}$$

is the absolute excitation cross section for those

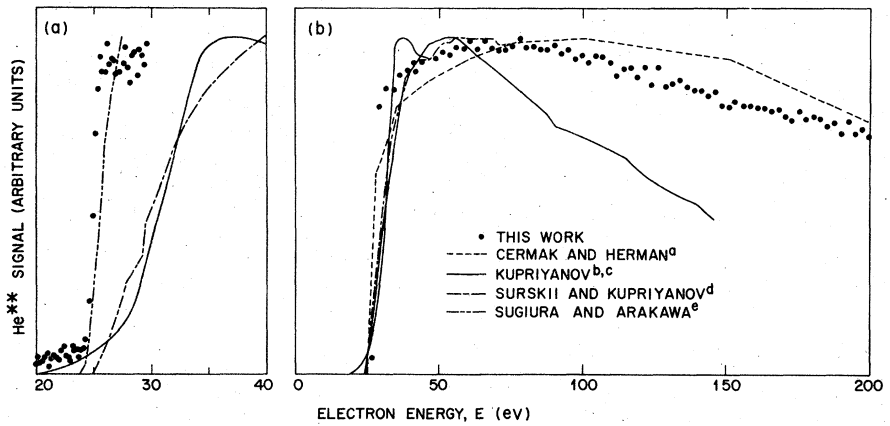


FIG. 7. He high Rydberg excitation functions measured in this work compared to those measured elsewhere. Threshold region is shown in (a) and higher-energy region in (b). In (b) the curves of other experimenters are plotted so that their thresholds agree with those measured in this work. The cited works are as follows (a) Ref. 16, (b) Ref. 17, (c) Ref. 18, (d) Ref. 20. and (e) Ref. 23.

fixed conditions. We can use Eq. (19) to measure $\sigma_T^{ex}$ from measurements of $\hat{I}_T$, $\eta$, $L$, $\Omega$, $\rho$, and $i$, provided the conditions for which Eq. (10) is applicable are maintained. Those conditions are that He pressure be kept low and electron current high. This insures that all detected HR atoms have suffered $\Delta l$ collisions, and that the collisions be only with electrons, as discussed in Sec. III C. To measure $\sigma_T^{ex}$, we must assume that the high Rydberg angular distribution is isotropic, which should be assured for an equilibrated gas.

The absolute excitation cross sections were measured without the analyzer plates in order to increase signal level. A 1.59-cm-diam aperture directly in front of the detector accurately defines a solid angle of $(4.9 \pm 0.5) \times 10^{-3}$ sr.

The pressure measurement procedure is to admit gas to the vacuum chamber at a point close to the diffusion pump and far from the interaction region, so that flow rates in the interaction region are small. A Baratron pressure gauge connected to the interaction region by 3-mm ID tubing is used at pressures from $10^{-5}$ to $10^{-4}$ Torr to calibrate an ionization gauge on the vacuum chamber. The ionization gauge is then used to measure pressures in the $\sim 10^{-6} - 10^{-5}$ Torr region with an estimated 40% uncertainty. It was found that all cross sections were independent of pressure below $3 \times 10^{-6}$ Torr, so all measurements were made below that pressure. To verify that gas flow does not lead to pressure differences between the ionization gauge and the interaction region, we checked all cross sections by measuring them with static gas (the gate valve closed). The values agreed with the flowing gas values, but with one complication: with no pumping, the partial pressure of water rose to $\sim 10^{-6}$ Torr. This was sufficient to collisionally ionize a large fraction of the HR atoms. The solution was to introduce a liquid nitrogen cooled cold trap into the chamber. This pumped $H_2O$ but not He.

The measurement procedure must account for detector counts $\hat{I}_T$ not due to high Rydbergs. Metastable states, as shown by Fig. 3, contribute no more than a few percent of the signal and so are ignored. uv photons, however, give count rates comparable to those for high Rydbergs. The procedure used is to determine from a time-of-flight measurement at the electron energy of interest what fraction of the total signal is due to high Rydbergs. The cross-section measurement is then made with the electron beam on continuously and the signal is corrected to give $\hat{I}_T$. The overall uncertainty in $\hat{I}_T$ including anisotropy, correction for photons, and counting statistics is an estimated 15%. The uncertainty in the $\sigma_T^{ex}$ measurement is determined largely by the 40% uncertainty in the gas density $\rho$. When we include uncertainties of the other factors in quadrature, the overall uncertainty becomes ±50%.

The measurement obtains $\sigma_T^{ex} = 3 \times 10^{-20}$ cm$^2$ for HR He atoms in our apparatus with $20 \leq n \leq 80$ and at $E = 100$ eV. This value for $\sigma_T^{ex}$ represents an average of many measurements at different pressures over the range $(1-3) \times 10^{-6}$ Torr and at $i = 30$ $\mu$A. We have also measured $\sigma_T^{ex}$ for different energies to check its value against the high Rydberg excitation function in Fig. 3(b).

With the measured value for $\sigma_T^{ex}$ and Eqs. (11) and (20), we can determine $\sigma^{ex}(n=1, E)$. Thus we find at 100 eV that

$$\sigma^{ex}(n, 100) = (9 \pm 5) \times 10^{-17}/n^3 \qquad (21)$$

independent of the particular apparatus. This expression predicts that for $n = 4$, $\sigma^{ex}(4, 100) = 1.4 \times 10^{-18}$ cm$^2$, which agrees with the optically measured value[33] of $1.2 \times 10^{-18}$ cm$^2$.

### D. High Rydberg collisions with electrons

This discussion, so far, has not considered collisions of high Rydbergs with other particles. What experimental evidence is there that collisions are significant?

The most striking evidence is that the radiative lifetimes for $nS$, $nP$, and $nD$ states, extrapolated from accurate low $n$ values,[47] are much too short to account for the $n$ distribution of Fig. 5, even though we expect only these low $l$ states to be populated by electron impact. The dashed curve in the lower right corner of Fig. 5(a) shows this calculated distribution. We conclude, therefore, that some mechanism lengthens the lifetimes of those high Rydbergs which do reach the detector. It appears that for sufficiently high $n$, the lifetimes of essentially all HR atoms are lengthened, since the $n = 4$ cross section extrapolated from the HR cross section (Sec. IV C) is in good agreement with the optically measured $n = 4$ value.[33] In addition, the $n = 4$ excitation function agrees with our high current, low pressure, HR excitation function [Fig. 3(b)], thus showing that most atoms *initially* excited to $^1P$ HR states have not radiated, despite their very short radiative lifetimes.

The proposed mechanism for lifetime lengthening, is increase of $l$ due to electron collisions with low-$l$ Rydberg atoms. According to Herrick's formulation[42] of critical angular momentum, $l_c$, the minimum $l$ which survives radiation and reaches the detector is given approximately by

$$l_c = 103.5(t_d/n^3)^{1/2} - 0.4\,, \qquad (22)$$

where $t_d$ has units of $\mu$sec. For example, $l_c \cong 8$ for $n = 25$ and $l_c \cong 3$ for $n = 45$. This formulation is

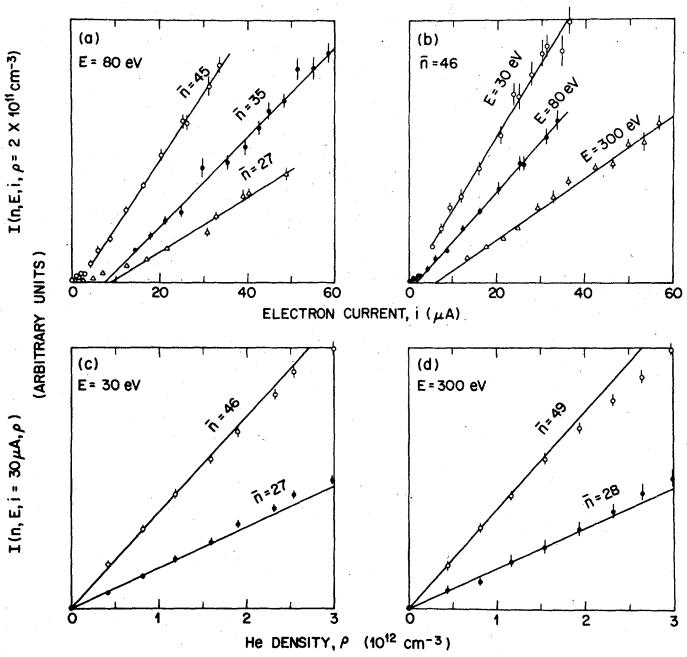


FIG. 8. He high Rydberg signals measured as a function of electron current (a and b) and gas density (c and d) with $\bar{n}$ and $E$ as parameters. The vertical scaling is chosen for clarity of the plots. Straight lines are drawn through the linear regions of a and b at high current, and through the origin and low-density points in c and d.

based on a simplified model of radiative lifetimes and so is of limited accuracy. It does however show that most initially excited atoms must undergo $l$ increases greater than unity in order to be detected. There is no present experimental evidence to show whether the entire increase results from collision with a single electron, or a series of collisions with different electrons. This question is left for further study.

The occurrence of $l$ increases caused by electron collisions implies that two (or more) electrons are required to produce a detected HR atom, and therefore that the signal should be proportional to the square of the electron current. Such behavior is implicit in Eq. (9) which has the form:

$$I(i) \propto \alpha i^2/(\alpha i+\beta)\,. \tag{23}$$

At low current $\alpha i \ll \beta$ so $I(i) \propto i^2$, but at high current $\alpha i \gg \beta$ so $I(i) \propto i$. Verification of this behavior is a necessary test of the multiple collision mechansim. Measurements are plotted in Fig. 8(a) and 8(b). Each set of data points exhibits linear behavior for $i \gtrsim 15$ $\mu$A. As predicted by Eq. (23), straight lines drawn through these points do not extrapolate to the origin, so the behavior must be nonlinear for low current.

Equation (23) and Figs. 8(a) and 8(b) can also be used to quantitatively determine $\sigma^e_{\Delta l}$. For $\alpha i \gg \beta$ Eq. (23) can be approximated by $I(i) \propto i - \beta/\alpha$ which is the equation for a straight line whose intercept with the $i$ axis is $i_0 = \beta/\alpha$. At He densities sufficiently low so that atomic $\Delta l$ collisions are negligible compared to electron $\Delta l$ collisions, $\beta/\alpha = Ae/\sigma^e_{\Delta l} t_p$ by comparison of Eq. (23) with Eq. (9). Thus by measurements of $i_0$ from straight lines through the linear regions of the data in Figs. 8(a) and 8(b), we can estimate $\sigma^e_{\Delta l}$ using

$$\sigma^e_{\Delta l} = Ae/i_0 t_p\,. \tag{24}$$

Table V gives $\sigma^e_{\Delta l}$ as derived from Eq. (24) and the data of Figs. 8(a) and 8(b). It can be seen that $\sigma^e_{\Delta l}$ increases with increasing $n$ and decreases with increasing $E$, consistent with Eq. (1).

An independent method of determining $\sigma^e_{\Delta l}$ is based on the variation of excitation functions with $\bar{n}$ [Fig. 6(a)]. This variation results primarily from competition between radiative decay of the short-lived $n\,^1P$ states and electron collisions which convert $^1P$ states to longer-lived states with

TABLE V. Cross section for $\Delta l$ caused by electron impact.

| $n$ | $\bar{n}$ | $E$ (eV) | $\sigma^e_{\Delta l}$ ($10^{-10}$ cm$^2$) From $I$-vs-$i$ measurements [a] | From $I$-vs-$E$ measurements [b] |
|---|---|---|---|---|
| 30–80 | 46 ± 4 | 30 | $80^{+\infty}_{-32}$ | $120^{+120}_{-60}$ |
| 30–80 | 45 ± 4 | 80 | $28^{+15}_{-7}$ | $42^{+42}_{-21}$ |
| 30–80 | 49 ± 4 | 300 | $7.8^{+1.6}_{-0.5}$ | $17^{+17}_{-9}$ |
| 20–30 | 27 ± 2 | 80 | $5.3^{+2.7}_{-0.5}$ | $5.2^{+5.2}_{-2.6}$ |
| 30–40 | 35 ± 3 | 80 | $6.4^{+2.4}_{-1.1}$ | $15^{+15}_{-8}$ |

[a] Equation (24).
[b] Equation (26).

higher $l$. If collisions take place rapidly enough, nearly all $^1P$ states will be converted to long-lived high-$l$ states and the resulting excitation function will be the sum of the $\sigma^{ex}$, such as that shown in Fig. 3(b). However, if the collision rate is slow, many $^1P$ atoms will radiate and the states which remain will be those having excitation functions which peak below 50 eV. Since the collision rate depends on $\sigma^e_{\Delta l}$, which varies as $n^4$, we should see different excitation functions for different $n$ ranges, just as in Fig. 6(a).

$\sigma^e_{\Delta l}$ has been determined from the data of Fig. 6(a) in the following way. Equation (9) is used to calculate an excitation function for an $n$-range equivalent to that for each of the measured excitation functions in Fig. 6(a). The pressure is low enough that $\sigma^e_{\Delta l} i/eA \gg \sigma^a_{\Delta l} \rho D/t_p$. $\sigma^{ex}$ is taken as

$$\sigma^{ex} = n^{-3}\sigma^{ex}_j(n=1,E) \tag{25}$$

where $\sigma^{ex}_j(n=4,E)$ is given by the measurements of Donohue *et al.*[33] Recall that $j$ signifies one of the $S$, $P$, or $D$ states of a given $n$. The form of $\sigma^e_{\Delta l}$ is given by Eq. (1). $\gamma$ can be calculated from a formula given by Herrick,[42] which shows that it ranges from 1 to $10^4$ eV$^{-1}$ for $l \leq 2$. $\gamma$ appears only logarithmically, however, and we find that varying it has little effect on the calculated excitation function. We have therefore fixed $\gamma$ at an intermediate value of 100 eV$^{-1}$. $K$ is now varied until the calculated excitation function best agrees with experiment. The result is that

$$\sigma^e_{\Delta l} \cong 5 \times 10^{-(1.5\pm0.3)} \ln(100En^2)n^4/E \text{ cm}^2, \tag{26}$$

where $E$ is in eV. The calculated excitation functions, plotted in Fig. 6(a), show acceptably good agreement with the measurements.

The accuracy of Eq. (26) is indicated by comparing the values of $\sigma^e_{\Delta l}$ determined by the two methods. Table V shows agreement within a factor of ~2, acceptable, we believe, in light of experimental uncertainties and the approximations inherent in the phenomenological model.

The large magnitude of $\sigma^e_{\Delta l}$ is emphasized by comparing its values with those for $\Delta n = \pm 1$ cross sections, calculated by Saraph[43]; the present values are approximately one order of magnitude larger. It thus appears that $\Delta n = \pm 1$ collisions, although not negligible, are relatively unimportant in this experiment.

The high probability of $l$-changing collisions found in this work should apply in any environment where high Rydbergs and electrons are both present. This applies to plasmas, discharges, interstellar space, and of course many previous laboratory experiments on high Rydbergs.

### E. High Rydberg collisions with ground-state atoms

The effects of collisions of HR atoms with ground-state atoms are seen in Figs. 5(b), 6(b), and 8(c), and 8(d). Higher pressures lead to an increase in the intensity of detected low $n$ Rydbergs [Fig. 5(b)]. Also, higher pressures change the excitation function shape to show less resemblance to the $^1P$ shape [Fig. 6(b)]. These observations can be explained by $l$-increasing collisions of low-$n$ ($n \lesssim 30$) Rydberg atoms before they reach the detector. For these low-$n$ Rydbergs, $\sigma^e_{\Delta l}$ is relatively small so at low pressure many of them radiate before reaching the detector. Atomic collisions along the flight path can transfer some of them to higher $l$ levels with longer lifetimes, thus increasing the low-$n$ signal. Since the $n^1P$ radiative lifetimes are so short, atomic collisions have a negligible effect on them, but $S$, $D$, and $^3P$ states are affected. Thus, the excitation function peak moves to low energy at high pressure [Fig. 6(b)].

The direct measurements of signal as a function of pressure [Figs. 8(c) and 8(d)] can be interpreted quantitatively by Eq. (8), although the weak signals and consequently noisy data preclude accurate results. Quenching collisions, represented by exp $(-\sigma^a_q \rho D)$, include ionization of the Rydberg atom and excitation transfer to ground-state atoms not headed toward the detector. The contribution of $T2$ (see Fig. 4) is the second term in the braces. It leads to an increase in signal at high pressures, as low-$l$ Rydberg atoms are collisionally transferred to longer-lived high-$l$ states. These two competing factors determine the curve shapes in data such as Figs. 8(c) and 8(d). The increase due to $T2$ is most obvious for $\bar{n} = 28$ in Fig. 8(d). Calculations of $I$ vs $\rho$, using Eq. (8), $\sigma^e_{\Delta l}$ from the preceding section, and values of experimental variables appropriate to Figs. 8(c) and 8(d) show that $\sigma^a_q = 40 \pm 20$ Å$^2$ and $\sigma^a_{\Delta l} = 200^{+200}_{-100}$ Å$^2$.

Although these cross sections do not refer to specific $l$ values, their magnitudes are reasonable. Recent measurements of atom-high Rydberg collision cross sections[13,48] (similar to $\sigma^a_{\Delta l}$) show that they should be roughly independent of $n$ or even decrease with increasing $n$ for $n \gtrsim 7$. The magnitude of this plateau value is found to be between 15 and 2000 Å$^2$ for various specific changes of $l$.

There are no experimental values of $\sigma^a_q$ for comparison. The cross section for ionization of high Rydbergs by collision with polar molecules[21,49] has been measured to be approximately $10^4$ Å$^2$, but that for ionization by collision with helium atoms has not been reported. The present upper limit of $40 \pm 20$ Å$^2$ is indeed small enough to have precluded detection in those previous experiments.

Resonant excitation transfer may indeed be the dominant contribution to that 40 Å$^2$.

### F. *l*-state mixing by electric fields

Electric fields can, of course, mix the $l$ states of an atom and so alter its radiative lifetime. Such an effect has been reported by Stebbings *et al.*[8] They found that a field of 25 V/cm increased the lifetime of the $25f$ states of Xe from 8 to 24 $\mu$s.

We have checked our measurements to verify that electric fields in the electron beam region are not important in producing our observed lifetime lengthening. Normally, the electric field in the excitation region is zero, since all nearby surfaces are grounded. There can of course be fields due to surface potentials, space charge, and penetration from the electron gun. An indication that the electric field is small is the sharpness of the measured threshold in Fig. 3(a); it is most likely that the magnitude of a stray field would be comparable to its inhomogeneity.

As a direct test, we introduced a field of ~20 V/cm into the excitation region and remeasured the $\bar{n}=26$ excitation function of Fig. 6(a). The result was very similar to the $\bar{n}=52$ curves, indicating that the electric field mixed $^1P$ states with higher $l$ states and so prevented their loss by radiation.

## ACKNOWLEDGMENTS

We thank G. J. Fisanick-Englot and W. Klemperer for helpful discussions.

*Present address: Dept. of Chemistry, University of Oregon, Eugene, Ore. 97403.

[1]R. N. Il'in, V. A. Oparin, I. T. Serenkov, E. S. Solov'ev, and N. V. Federenko, Zh. Eksp. Teor. Fiz. 59, 103 (1970) [Sov. Phys.-JETP 32, 59 (1971)].
[2]R. N. Il'in, in *Atomic Physics 3*, edited by S. J. Smith and G. K. Walters (Plenum, New York, 1973), p. 309
[3]J. E. Bayfield, G. A. Khayrallah, and P. M. Koch, Phys. Rev. A 9, 209 (1974).
[4]F. A. Jenkins and E. Segrè, Phys. Rev. 55, 52 (1939).
[5]W. R. S. Garton and F. S. Tomkins, Astrophys. J. 158, 1219 (1969).
[6]G. Herzberg and C. Jungen, J. Mol. Spectrosc. 41, 425 (1972).
[7]P. M. Dehmer and W. A. Chupka, J. Chem. Phys. 65, 2243 (1976).
[8]R. F. Stebbings, C. J. Latimer, W. P. West, F. B. Dunning, and T. B. Cook, Phys. Rev. A 12, 1453(1975).
[9]W. P. West, G. W. Foltz, F. B. Dunning, C. J. Latimer, and R. F. Stebbings, Phys. Rev. Lett. 36, 854 (1976).
[10]R. F. Stebbings, Science 193, 537 (1976).
[11]T. F. Gallagher, S. A. Edelstein, and R. M. Hill, Phys. Rev. Lett. 35, 644 (1975).
[12]T. F. Gallagher, S. A. Edelstein, and R. M. Hill, Phys. Rev. A 11, 1504 (1975); 14, 2360 (1976).
[13]T. F. Gallagher, R. M. Hill, and S. A. Edelstein, Phys. Rev. A 13, 1448 (1976); 14, 744 (1976).
[14]T. W. Ducas, M. G. Littman, R. R. Freeman, and D. Kleppner, Phys. Rev. Lett. 35, 366 (1975).
[15]M. G. Littman, M. L. Zimmerman, T. W. Ducas, R. R. Freeman, and D. Kleppner, Phys. Rev. Lett. 36, 788 (1976).
[16]V. Čermák and Z. Herman, Collect. Czech. Chem. Commun. 29, 953 (1964).
[17]S. E. Kupriyanov, Zh. Eksp. Teor. Fiz. 48, 467 (1965) [Sov. Phys.-JETP 21, 311 (1965)].
[18]S. E. Kupriyanov, Opt. Spektrosk. 20, 163 (1966) [Opt. Spectrosc. 20, 85 (1966)].
[19]S. E. Kupriyanov, Zh. Eksp. Teor. Fiz. 55, 460 (1968) [Sov. Phys.-JETP 28, 240 (1969)].
[20]G. A. Surskiĭ and S. E. Kupriyanov Zh. Eksp. Teor. Fiz. 54, 109 (1968) [Sov. Phys.-JETP 27, 61 (1968)].
[21]H. Hotop and A. Niehaus, J. Chem. Phys. 47, 2506 (1967).
[22]H. Hotop and A. Niehaus, Z. Phys. 215, 395 (1968).
[23]T. Sugiura and K. Arakawa, *Recent Developments in Mass Spectroscopy*, edited by K. Ogata and T. Hayakawa (Univ. of Tokyo Press, Tokyo, 1970), p. 848.
[24]R. S. Freund, J. Chem. Phys. 54, 3125 (1971).
[25]K. C. Smyth, J. A. Schiavone, and R. S. Freund, J. Chem. Phys. 59, 5225 (1973).
[26]K. C. Smyth, J. A. Schiavone, and R. S. Freund, J. Chem. Phys. 60, 1358 (1974).
[27]J. A. Schiavone, K. C. Smyth, and R. S. Freund, J. Chem. Phys. 63, 1043 (1975).
[28]W. L. Borst and E. C. Zipf, Phys. Rev. A 4, 153 (1971).
[29]T. G. Finn, B. L. Carnahan, W. C. Wells, and E. C. Zipf, J. Chem. Phys. 63, 1596 (1975).
[30]W. C. Wells, W. L. Borst and E. C. Zipf, Phys. Rev. A 14, 695 (1976).
[31]T. Shibata, T. Fukuyama, and K. Kuchitsu, Bull. Chem. Soc. Jpn. 47, 2883 (1974).
[32]M. Matsuzawa, J. Electron Spectrosc. Rel. Phenom. 4, 1 (1974).
[33]D. E. Donohue, J. A. Schiavone, and R. S. Freund (unpublished).
[34]R. S. Freund, Rev. Sci. Instrum. 41, 1213 (1970).
[35]S. E. Kupriyanov, Zh. Eksp. Teor. Fiz. Pis'ma Red. 5, 245 (1967) [JETP Lett. 5, 197 (1967)].
[36]A. V. Chaplik, Zh. Eksp. Teor. Fiz. 54, 332 (1968) [Sov. Phys.-JETP 27, 178 (1968)].
[37]W. L. Borst, Phys. Rev. A 9, 1195 (1974).
[38]U. Fano, J. Phys. B 7, L401 (1974).
[39]V. I. Ochkur, Zh. Eksp. Teor. Fiz. 45, 734 (1963) [Sov. Phys.-JETP 18, 503 (1964)].
[40]M. J. Seaton, Proc. Phys. Soc. 79, 1105 (1962).
[41]R. M. Pengelly and M. J. Seaton, Mon. Not. R. Astron. Soc. 127, 165 (1964).
[42]D.R. Herrick (unpublished).
[43]H.E. Saraph, Proc. Phys. Soc. 83, 763 (1964).
[44]L.C. Green, N. C. Johnson, and E. K. Kolchin, Astrophys. J. 144, 369 (1966).
[45]D. R. Herrick, J. Chem. Phys. 65, 3529 (1976).
[46]M. Gailitis and R. Ya. Damburg, Proc. Phys. Soc.

Lond. 82, 192 (1963).
[47]Derived from Ref. 44.
[48]R. S. Freund, T. A. Miller, B. R. Zegarski, R. Jost, M. Lombardi, and A. Dorelon (unpublished).
[49]W. A. Chupka, as quoted by M. Matsuzawa, Int. J. Mass Spectron. Rel. Phenom. 4, 1 (1974); Ref. 19.
[50]A. C. Riviere and D. R. Sweetman, in *Proceedings of the Sixth International Conference on Ionization Phenomena in Gases, Paris, 1963,* edited by P. Hubert (SERMA, Paris, 1964), Vol. 1, p. 105.